

Impact of Fibrinogen, Fibrin Thrombi, and Thrombin on Cancer Cell Extravasation Using In Vitro Microvascular Networks

Emmanouil Angelidakis, Sophia Chen, Shun Zhang, Zhengpeng Wan, Roger D. Kamm,* and Sarah E. Shelton*

A bidirectional association exists between metastatic dissemination and the hypercoagulable state associated with many types of cancer. As such, clinical studies have provided evidence that markers associated with elevated levels of coagulation and fibrinolysis correlate with decreased patient survival. However, elucidating the mechanisms underpinning the effects of different components of the coagulation system on metastasis formation is challenging both in animal models and 2D models lacking the complex cellular interactions necessary to model both thrombosis and metastasis. Here, an in vitro, 3D, microvascular model for observing the formation of fibrin thrombi is described, which is in turn used to study how different aspects of the hypercoagulable state associated with cancer affect the endothelium. Using this platform, cancer cells expressing ICAM-1 are shown to form a fibrinogen-dependent bridge and transmigrate through the endothelium more effectively. Cancer cells are also demonstrated to interact with fibrin thrombi, using them to adhere, spread, and enhance their extravasation efficiency. Finally, thrombin is also shown to enhance cancer cell extravasation. This system presents a physiologically relevant model of fibrin clot formation in the human microvasculature, enabling in-depth investigation of the cellular interactions between cancer cells and the coagulation system affecting cancer cell extravasation.

1. Introduction

Cancer-associated thrombosis (CAT), or Trousseau's syndrome, is the second leading cause of death among cancer patients, following metastatic spread.^[1] Clinical manifestations include venous thromboembolism (VTE), arterial thrombosis, and disseminated intravascular coagulation (DIC).^[2] In a Danish population-based study, VTE risk was about six times higher in stage IV cancer patients compared to stage I patients.^[3] DIC was also shown to be significantly more prominent among advanced stage cancer patients.^[4] Furthermore, clinical studies have shown that elevated levels of several components of the coagulation system are correlated with decreased patient survival and poor prognosis in many types of cancer. Edwards et al. showed that in a cohort of patients with lung, colorectal, prostate, and head and neck carcinoma, fibrinogen levels steadily increased prior to death.^[5] Another study found that increased blood D-dimer levels, a product of fibrin degradation and a proxy


of hemostasis and fibrinolysis activation, is associated with increased mortality risk.^[6]

The coagulation system consists of blood cells and proteins responsible for blood clotting, platelet activation and repair of damaged blood vessels. Upon endothelial damage, tissue factor (TF) expressed in the subendothelium triggers a cascade of reactions, which culminate in the formation of a platelet plug (primary hemostasis) and the formation of a fibrin clot (secondary hemostasis). Activated platelets aggregate on the site of injury forming a platelet plug, while exposed TF forms a complex with factor VII which results in thrombin generation.^[7] Thrombin then cleaves fibrinopeptides A and B from fibrinogen, inducing polymerization of fibrin fibers.^[8] In parallel, platelets bind to fibrin, contracting adjacent fibers to form tightly packed thrombi.^[9] Platelets further interact with and recruit immune cells to the site of injury, including facilitating leukocyte extravasation^[10] and monocyte-to-macrophage differentiation.^[11] Under pathological conditions, including malignancy, the coagulation system can become abnormally activated, clinically manifested as CAT.^[12] In addition, evidence suggests that different components of the

E. Angelidakis, S. Chen, S. Zhang, Z. Wan, R. D. Kamm, S. E. Shelton
Department of Biological Engineering
Massachusetts Institute of Technology
Cambridge, MA 02139, USA
E-mail: rdkamm@mit.edu; sshelton@mit.edu

R. D. Kamm
Department of Mechanical Engineering
Massachusetts Institute of Technology
Cambridge, MA 02139, USA

S. E. Shelton
Department of Medical Oncology
Dana Farber Cancer Institute
Boston, MA 02215, USA

 The ORCID identification number(s) for the author(s) of this article can be found under <https://doi.org/10.1002/adhm.202202984>

© 2023 The Authors. Advanced Healthcare Materials published by Wiley-VCH GmbH. This is an open access article under the terms of the Creative Commons Attribution-NonCommercial License, which permits use, distribution and reproduction in any medium, provided the original work is properly cited and is not used for commercial purposes.

DOI: 10.1002/adhm.202202984

coagulation system interact with circulating tumor cells and impact cancer cell extravasation and metastasis formation.

Hematogenous metastasis is the process through which cancer cells in the primary tumor invade surrounding tissue, intravasate into nearby blood vessels, transit through the circulation, extravasate into distant tissues, and start colonizing them, eventually forming metastases (secondary tumors).^[13] Once in circulation, cancer cells heavily interact with the coagulation system. In fibrinogen-deficient mice, melanoma cells formed significantly fewer lung metastases following intravenous injection.^[14] In platelet-deficient mice, the median lung tumor count two weeks after melanoma cell injection was 6% that of wild type.^[15] Furthermore, tumor-cell associated TF was shown to protect circulating tumor cells from natural killer cell-mediated lysis in a fibrinogen-dependent manner.^[16] These studies provide concrete evidence that the coagulation system plays a key role in metastatic dissemination. However, they have provided limited insight into the mechanisms underpinning the interactions between the coagulation system and cancer cells, and how in turn these mechanisms facilitate metastasis formation. In addition, animal studies are time- and labor-intensive, present difficulties in parametrization, and do not necessarily translate to human pathophysiology due to interspecies differences.

One approach to better understand the interactions between the coagulation system and cancer cells is to use a physiologically relevant *in vitro* model of human vasculature and thrombus formation. One example is that of Zheng et al., in which the authors used a soft lithography platform to develop *in vitro* microvessels which they then used to study blood-endothelium interactions upon phorbol-12-myristate-13-acetate (PMA) activation.^[17] While this study provided insights into platelet aggregation in a prothrombotic state of the endothelium, there was no investigation of secondary hemostasis. In another example, Zhang et al. used 3D bioprinting to generate an endothelialized lumen, where a thrombus was formed via whole blood perfusion.^[18] They then demonstrated that the thrombus could be resolved by perfusion of tissue plasminogen activator, a clinical thrombolytic agent. In addition, Sakurai et al. generated a microfluidic bleeding model, which captured aspects of both phases of hemostasis, further demonstrating that platelet-dependent clot contraction can be pharmacologically modulated, while also showing *in vitro* that platelet dynamics are shear-dependent.^[19] While these studies have offered insights into the nature of thrombus formation, the models developed lack the morphological complexity of native capillary beds which can potentially affect the ways thrombi form and behave, as well as the ways in which cancer cells adhere to the endothelium and extravasate. Furthermore, a model recapitulating the morphological diversity of native capillary beds would allow cancer cells to become physically trapped in the vessels of smaller diameter, recapitulating both proposed adherence mechanisms taking place *in vivo*.^[20,21]

To address the main limitations of previous models, here we used a microfluidic model where endothelial and stromal cells seeded in a fibrin gel self-assemble to form microvascular networks, as a model of the human lung microvasculature. This platform is in turn used to generate and characterize fibrin thrombi, investigate the interactions of fibrin and thrombin with the endothelium and finally evaluate how these components affect cancer cell extravasation. We find that both fibrin clot formation and

thrombin treatment impair endothelial barrier function. Using this platform, we find that breast cancer cells expressing ICAM-1 can enhance their extravasation in a fibrinogen-dependent manner, and that the presence of fibrin thrombi in the microvascular networks enhances cancer cell retention, and in turn adhesion and extravasation. Additionally, thrombin treatment also enhances breast cancer cell extravasation, independent of fibrin(ogen). Our system represents a physiologically relevant *in vitro* model of human lung microvasculature, used to model the hypercoagulable state in cancer to investigate how it affects the endothelium and how fibrinogen, fibrin thrombi, and thrombin influence breast cancer cell extravasation.

2. Results

2.1. *In Vitro* Model of Fibrin Clot Formation Using Microvascular Networks

Microvascular networks were generated according to previously established protocols of our group.^[22] Briefly, endothelial cells and lung fibroblasts were seeded in a fibrin gel, self-assembling to form perfusable microvascular networks within a week. Then, fibrin clots were generated by perfusing recalcified human plasma spiked with fluorescent fibrinogen, diluted in human plasma-like medium (**Figure 1a**). Thrombi formed and stabilized within fifteen minutes following perfusion (**Figure S1**, Supporting Information), at which point the plasma solution was replaced with endothelial culture medium. A range of plasma concentrations was used (**Figure 1b**), producing a graded response with respect to % fibrin⁺ vessel area (**Figure 1c**). With higher plasma concentrations, the fibrin clots increasingly occupy the intravascular space, forming denser and more extensive clots (**Figure 1b**). This is also reflected in the increasing % fibrin⁺ vessel area, reaching up to $\approx 20\%$ for the highest plasma concentration investigated (**Figure 1c**). To further demonstrate the potential of this platform, we perfused platelet-rich plasma through the networks. Clots formed made up of both fibrin and platelets, as stained by CD41 (**Figure 1d**, lower panel). Platelets are entangled in fibrin clots, showing similar strand-like patterns as seen in fibrin clots lacking platelets (**Figure 1b**). Von Willebrand factor (vWF), with a key role in platelet adhesion,^[23] can further be seen in the clots (upper panel). Nevertheless, platelets were not examined further in this study, and all subsequent experiments were performed using plasma only, focusing on secondary hemostasis (fibrin(ogen)/thrombin). In addition, the flow-driven patterns seen (**Figure 1b,d**, transient flow is introduced from left to right using a pressure difference across the networks) exemplify why network geometry is relevant to thrombus formation.

To determine whether the clots formed occluded segments of the microvascular networks, 1 μm -diameter fluorescent beads were perfused following clot formation using 25% and 50% plasma concentration (**Figure 2a**, plus additional whole-device images in **Figure S2a**, Supporting Information). There are clearly occluded segments of the microvascular networks through which the 1 μm beads cannot pass, suggesting that red blood cells and platelets with average diameters of 7–8 and 1.5–3 μm , respectively,^[24] would accumulate in those regions if whole blood were used for the experiments. However, we also observed that there were no occlusions present 24 h after plasma perfusion

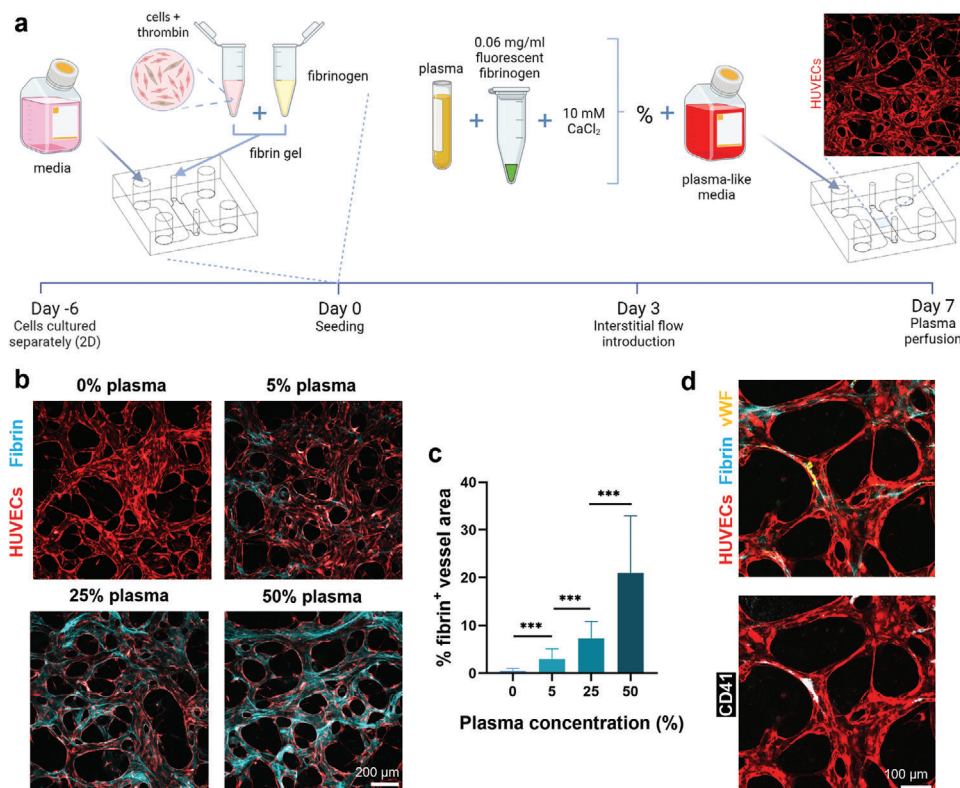


Figure 1. Generation of in vitro microfluidic model of fibrin clot formation. a) Experimental setup and timeline. Human umbilical vein endothelial cells (HUVECs) and normal human lung fibroblasts (NHLFs) were seeded in a fibrin gel where they self-assembled to form microvascular networks, within a week. Recalcified plasma was then perfused to form fibrin clots. b) Representative images of microvascular networks and fibrin clots at different plasma concentrations. Scale bar 200 μm. c) Quantification of % fibrin⁺ vessel area for different plasma concentrations ($n = 20$, 2 independent experiments). Data analyzed by Mann–Whitney U test. d) Representative images of clots in microvascular networks upon perfusion of recalcified platelet-rich plasma (25% in PBS), including fibrin (cyan) and von Willebrand factor (vWF, yellow) (upper panel) and platelets (white, stained for CD41) (lower panel). Scale bar: 100 μm. Each datum point represents a single ROI. Bars represent mean \pm SD. *** $P < 0.001$. Statistical analyses are described in the Experimental Section.

and clot formation. To verify this, fluorescent beads were again perfused through the networks (Figure 2b, additional whole-device images at the latter timepoint are presented in Figure S2b, Supporting Information). Previously occluded segments became accessible to the beads within this timeframe, a phenomenon that could be due to either contraction of the fibrin clots or degradation. Clot contraction is a mechanism with roles in reinforcing hemostasis and restoring flow past otherwise occlusive thrombi.^[25] However, in vivo, platelets mediate this process by contracting fibrin fibers and compacting erythrocytes, forming tightly packed thrombi.^[25] The data presented here suggest that motor-free contraction could also take place in fibrin networks, in parallel to platelet-mediated contraction. Such motor-free contraction of biopolymer networks has previously been observed in budding yeast and *Drosophila* embryos, in myosin-independent contraction of the actomyosin ring during cytokinesis.^[26,27] Chen et al. have proposed a model of motor-free contractility of biopolymer networks, applying to viscoelastic substrates that exhibit nonlinear force-extension behavior.^[28] Fibrin being a nonlinear viscoelastic polymer,^[29] the proposed model could explain the contraction seen here. Alternatively, contraction of fibrin clots generated in plasma could be attributed to deswelling due to the release of proteins and lipids initially entrapped in the matrix.^[30]

Our system enables decoupling of the platelet-dependent and -independent fibrin contraction mechanisms to investigate their relative contributions to clot contraction in vivo. Quantitative assessment of the clots further revealed that the % fibrin⁺ vessel area significantly decreased within 24 h, while the fluorescent intensity of the areas in question significantly increased, further supporting the claim that fibrin fibers contracted (Figure 2c,d). This phenomenon can be seen more clearly in higher magnification images (Figure 2e). Clots occupy most of the vessel lumens within minutes after formation, as shown in the inset in the left panel, where it appears that there are long fiber segments filling the lumens. However, 24 h after introducing plasma, significantly more intravascular space is open, and the fibrin attachments to the endothelium can be clearly seen (Figure 2e, right panel). The interactions of fibrin with the endothelium and the space it occupies at the two timepoints can also be seen in 3D reconstructions of the z-stacks (Figure S3, Supporting Information). Besides contraction, we cannot exclude the possibility that fibrin degradation also takes place. Plasminogen, the zymogen precursor of plasmin that degrades fibrin during physiologic clot dissolution, is mainly produced by hepatocytes. While extrahepatic sites of synthesis have been identified,^[31] it is unlikely to be present in our system, especially since plasma solutions are

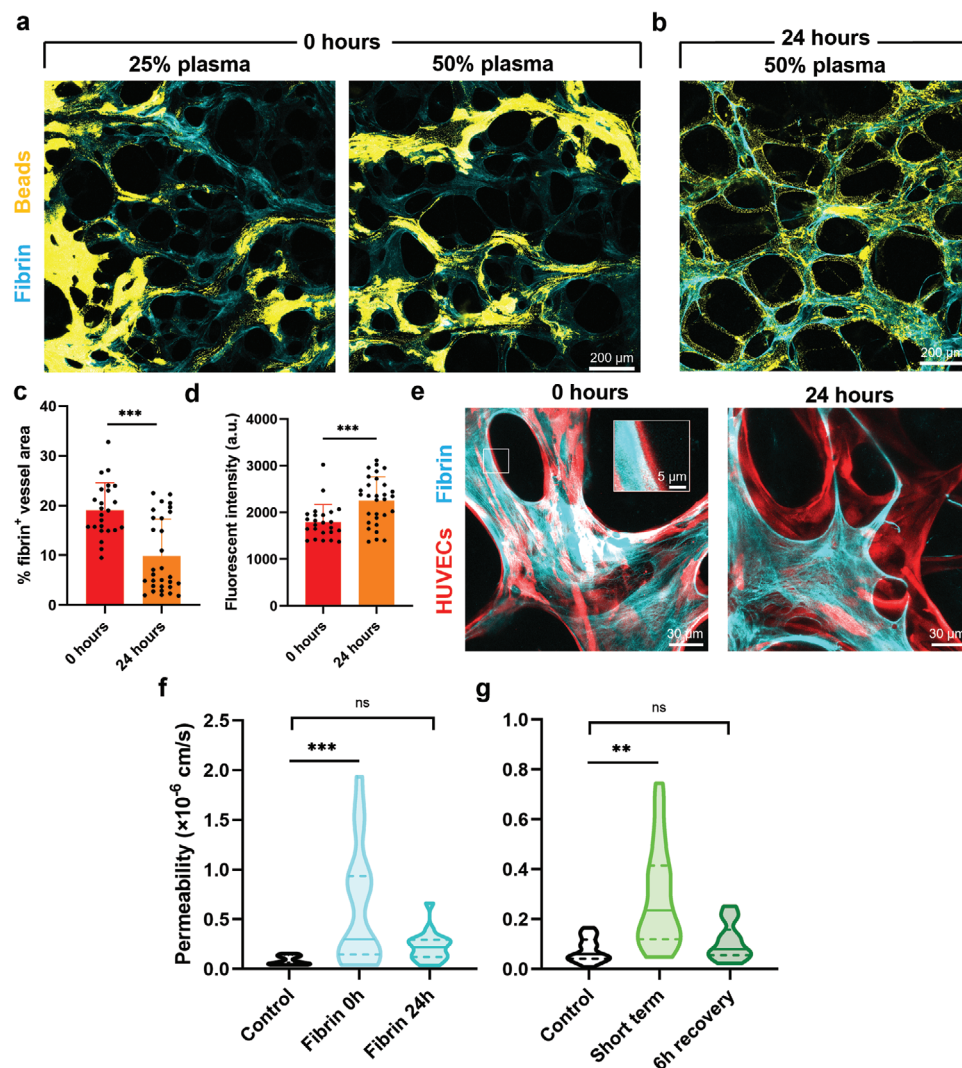


Figure 2. Interactions of fibrin and thrombin with microvascular networks. a) Representative confocal images of fibrin clots following fluorescent bead perfusion, right after clot formation (0 h). Microvascular networks not shown for clarity, scale bar: 200 μm . b) Representative confocal image of fibrin clots 24 h after formation, following perfusion of fluorescent beads. Scale bar: 200 μm . c,d) Quantification of % fibrin⁺ vessel areas and fluorescent intensity of those areas at same timepoints, using 25% plasma ($n = 24\text{--}30$, 2 independent experiments). Data analyzed by Mann–Whitney U test. e) High-magnification images of fibrin clots at two timepoints, using 50% plasma. Scale bar: 30 μm , inset 5 μm . f) Effect of fibrin on endothelial permeability. Endothelial permeability to 70 kDa dextran determined in control networks, networks immediately after formation of fibrin clots using 25% plasma, and 24 h following clot formation ($n = 17\text{--}18$, 2 independent experiments). g) Effect of thrombin on endothelial permeability, either immediately following treatment with 1 U mL^{-1} of thrombin for 1 h, or by treatment with 1 U mL^{-1} thrombin for 1 h followed by 6 h of control medium ($n = 26\text{--}47$, 3 independent experiments). Permeability data analyzed by one-way ANOVA with Tukey's post hoc analysis for multiple comparisons. Each datum point represents a single ROI. Bars represent mean \pm SD. In violin plots, midline indicates median, horizontal lines above and below indicate lower and upper quartiles. ns stands for not significant; ** $P < 0.01$; *** $P < 0.001$. Statistical analyses are described in the Experimental Section.

replaced with culture medium in the microvascular networks following clot formation. However, several matrix metalloproteinases, including 1, 2, 3, and 14, all of which can be produced by human umbilical vein endothelial cells (HUVECs),^[32–34] have been reported to have fibrinolytic activity^[35] and could potentially degrade the fibrin clots—the observations made could be the result of both fiber contraction and degradation.

To further characterize our system, we sought to investigate how fibrin clot formation affects endothelial permeability (Figure 2f). Fluorescently labeled dextran was perfused through the microvascular networks and its leakage through the endothe-

lium was quantified (Figure S4, Supporting Information). Initially, the endothelial permeability of untreated control networks was $\approx 1 \times 10^{-7} \text{ cm s}^{-1}$, in close agreement with previously reported values.^[36] Immediately after clot formation, there was a significant increase in permeability. Literature suggests that this may be a result of an interaction of fibrin with VE-cadherin, which leads to the disruption of homophilic cadherin interactions between adjacent endothelial cells that regulate endothelial permeability.^[37] Following activation of the coagulation cascade, thrombin cleaves fibrinopeptide B from fibrinogen, exposing a cryptic VE-cadherin binding site on fibrin adjacent to the

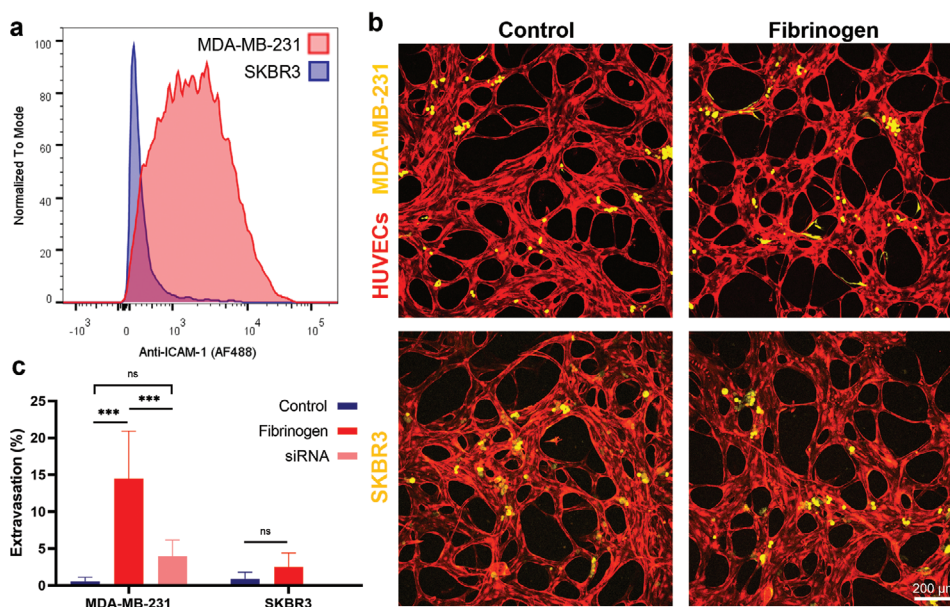


Figure 3. Effects of fibrinogen on cancer cell extravasation. a) Detection of ICAM-1 on the surface of SKBR3 and MDA-MB-231 cells, isotype control histograms not shown. b) Representative confocal images of SKBR3 and MDA-MB-231 cells perfused through the microvascular networks, at 24 h. Scale bar: 200 μm . c) Quantification of % extravasated cells in each cell line and condition (3 mg mL^{-1} fibrinogen, $n = 6-21$, 1–5 independent experiments). To inhibit the interaction between fibrinogen and ICAM-1, the networks were treated overnight with an anti-ICAM-1 blocking antibody (10 $\mu\text{g mL}^{-1}$), and the cancer cells were treated with a siRNA against ICAM-1 for 48 h prior to perfusion. Data analyzed by one-way ANOVA with Tukey's post hoc analysis for multiple comparisons (MDA-MB-231) and Student's t -test (SKBR3). Each datum point represents an individual device, with three ROIs imaged per device. Bars represent mean \pm SD. ns stands for not significant; *** $P < 0.001$. Statistical analyses are described in the Experimental Section.

cleavage site.^[37] This interaction leads to disruption of adherens junctions between adjacent endothelial cells,^[38] which would allow increased flux of dextran across the endothelium (Figure 2f). Twenty-four hours later, endothelial permeability decreased to control levels. To confirm that fibrinopeptide B cleavage is required to mediate the increase in endothelial permeability seen, we further perfused citrated plasma without recalcification in the microvascular networks. In the absence of Ca^{2+} ions, the coagulation cascade was not activated, therefore maintaining intact fibrinogen. In this case, no increase in endothelial permeability was observed (Figure S5, Supporting Information).

In addition, thrombin is known to induce endothelial hyperpermeability, acting through protease-activated receptor-1 (PAR-1) to disrupt the VE-cadherin/catenin complex and reorganize adherens junctions between adjacent cells.^[39] We therefore sought to determine whether this can also be recapitulated in our system (Figure 2g, with confocal images associated with quantification presented in Figure S6, Supporting Information). One hour of treatment with thrombin was sufficient to mediate a significant increase in endothelial permeability, which however recovered to control levels within 6 h in culture medium, as previously reported.^[39]

2.2. Interactions between Fibrinogen and Cancer Cells

Using this model, we then went on to investigate how fibrinogen and fibrin clots interact with cancer cells and affect their extravasation rate. The physiological range of fibrinogen in the blood of healthy individuals is 2–4 mg mL^{-1} .^[40] However, systemic

inflammation, present in many types of cancer,^[41] often leads to upregulated blood levels of IL-6,^[42,43] which in turn stimulates fibrinogen production from the liver.^[44] Besides this source, evidence shows that some cancer cell lines can produce fibrinogen themselves, suggesting that primary tumors can further contribute to pathologically elevating fibrinogen blood levels.^[45] In addition, elevated blood fibrinogen correlated with worse prognosis and increased metastasis formation in liver,^[46] stomach,^[47] and lung cancer^[48] patients in clinical studies. Mechanistically, a recent study demonstrated that pancreatic cancer cells can take advantage of an ICAM-1-fibrinogen-ICAM-1 bridge to adhere to and facilitate their extravasation through the endothelium.^[49] We therefore asked whether the same mechanism can be exploited by other types of cancer cells in our system. We selected MDA-MB-231 and SKBR3, two breast cancer lines with high and low ICAM-1 expression, respectively.^[50] The expression levels of the receptor on the cell surface of each cell line were first confirmed using flow cytometry (Figure 3a). Both cell lines were then perfused through the microvascular networks, in the presence or absence of 3 mg mL^{-1} fibrinogen in the culture medium (Figure 3b), and the extravasation rates were quantified 24 h after perfusion (Figure 3c). In the presence of fibrinogen (Figure 3b), MDA-MB-231 cells appear more elongated, likely due to forming more attachments to the endothelium. In the absence of fibrinogen however, most of them remain round. By 24 h, a significantly higher fraction has extravasated when fibrinogen is present (Figure 3c). Inhibiting the interaction of fibrinogen with ICAM-1 using a blocking antibody against endothelial ICAM-1 and a silencing RNA (siRNA) against ICAM-1 on the surface of MDA-MB-231 cells resulted in a significantly

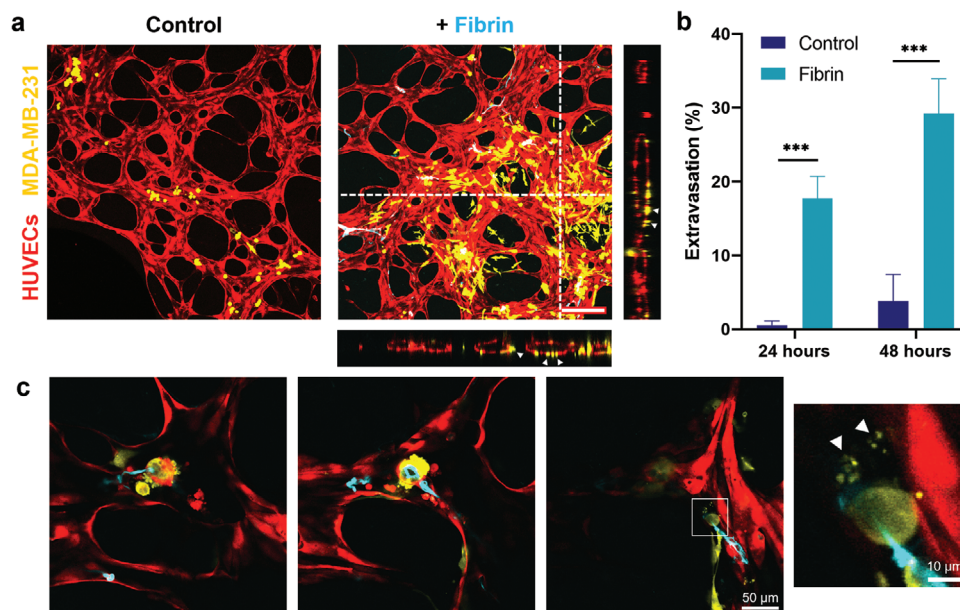


Figure 4. Effects of fibrin on cancer cell extravasation. a) Representative confocal images of MDA-MB-231 cells perfused through the microvascular networks in the absence or presence of fibrin clots (10% plasma) at 48 h. Dotted lines in fibrin panel indicate positions of XZ and YZ planes. White arrows in orthogonal views point to cancer cells adhering to the external wall of the endothelium following extravasation. Scale bar: 200 μm . b) Quantification of % extravasated cells in the two conditions ($n = 5\text{--}20$, 2–5 independent experiments). Each datum point represents an individual device, with three ROIs imaged per device. Data analyzed by Mann–Whitney U test. c) High-magnification confocal images of cancer cells interacting with fibrin clots. White arrows in inset of third image indicate cancer cell-derived microparticles. The images shown are different z positions of the same ROI, moving upward from left to right. Scale bar: 50 μm , inset 10 μm . Bars represent mean \pm SD. *** $P < 0.001$. Statistical analyses are described in the Experimental Section.

reduced extravasation rate over 24 h. Nonetheless, the response to fibrinogen seen in SKBR3 cells, which express little ICAM-1 (Figure 3a) is much less pronounced. SKBR3 cells appear mostly round in both conditions, with a very low fraction of them extravasated at 24 h. The data shown here suggest that breast cancer cell lines highly expressing ICAM-1 can take advantage of the ICAM-1-fibrinogen-ICAM-1 bridge to extravasate in our system.

Apart from facilitating the physical interaction between cancer cells and the endothelium, binding of fibrinogen to endothelial ICAM-1 could trigger further signaling events enhancing cancer cell extravasation. Studies have linked ICAM-1-mediated adhesion to increases in endothelial permeability,^[51] as well as increased proinflammatory signaling.^[52] These mechanisms could facilitate transmigration of the cancer cells through the endothelium. Finally, fibrinogen-mediated cancer cell adhesion to the endothelium could be another hallmark of the increasing prevalence of the liver as a metastatic site, in addition to its fenestrated endothelium, given its pivotal role in fibrinogen production.^[53]

2.3. Interactions between Fibrin Thrombi and Cancer Cells

Next, we sought to investigate the interactions of cancer cells with fibrin thrombi and their impact on extravasation. Clinical reports have shown that D-dimers, a fibrin degradation product and by extension a proxy of increased hemostasis and fibrinolysis activation, are significantly elevated in stage III and IV cancer patients compared to stages I and II.^[54] Furthermore, DIC, characterized by systemic activation of coagulation and excessive deposition of

fibrin in the vasculature of different organs, is correlated with lower patient survival at all cancer stages in a clinical study, while it was also significantly more prominent among patients with metastases.^[4] To date, there has been little research into the interactions of cancer cells with fibrin clots, even less so in the context of cancer cell extravasation. Knowles et al. demonstrated that cancer cell lines metastasizing preferentially to the lungs in mice can interact with fibrin clots through fibronectin complexed in them,^[55] mediated by activated integrin $\alpha_v\beta_3$ which coordinates the formation of invadopodia.^[56] However, besides these studies, there is limited research into the mechanisms through which fibrin thrombi affect cancer cell extravasation.

Therefore, we sought to investigate how MDA-MB-231 cells interact with fibrin clots in our model, and how this interaction subsequently impacts extravasation efficiency. Cancer cells were perfused together with 10% recalcified plasma in the microvascular networks and cultured up to 48 h. The presence of fibrin clots strongly influences the behavior of cancer cells (Figure 4a). Many cancer cells appear elongated, spreading on the endothelium, attaching to both internal and external walls, as shown in the orthogonal views on the right image (white arrows). These interactions can be more clearly seen in higher magnification images (Figure 4c). It appears that the cells can form attachments to fibrin, which could also be mediated by fibronectin entangled in the clots. Furthermore, the presence of fibrin significantly increases the rate of cancer cell extravasation (Figure 4b). In addition, cancer cell-derived microparticles were observed in the vicinity of some cancer cells (Figure 4c, white arrows in fourth image), known to activate the coagulation system and enhance cancer cell extravasation.^[57,58]

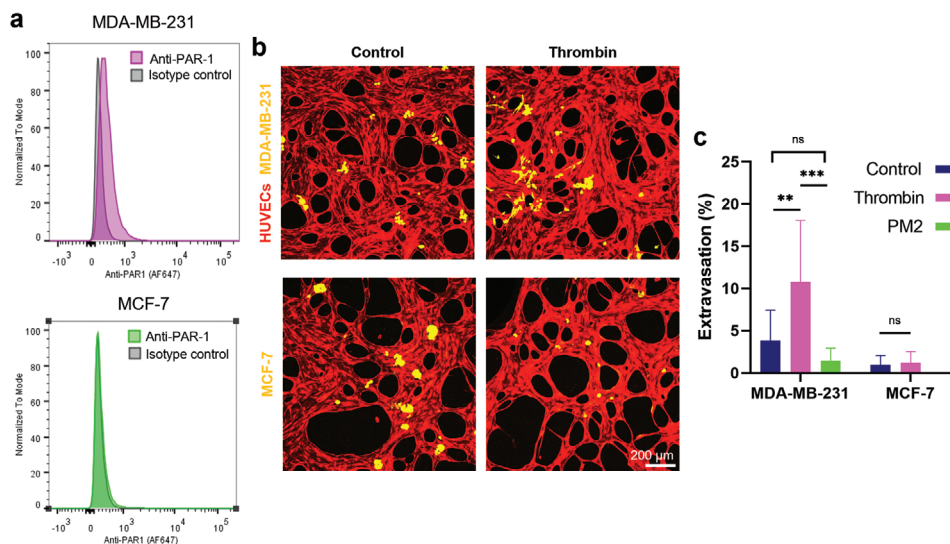


Figure 5. Effects of thrombin on cancer cell extravasation. a) Detection of PAR-1 on the surface of MDA-MB-231 and MCF-7 cells. b) Representative confocal images of two cell lines perfused through the microvascular networks with or without 4 U mL^{-1} thrombin at 48 h. Scale bar: $200 \mu\text{m}$. c) Quantification of % extravasated cells in each cell line and condition ($n = 9\text{--}19$, 2–5 independent experiments). When PM2 was used to inhibit PAR-1, both networks and cancer cells were treated ($30 \times 10^{-6} \text{ M}$) for 4 h prior to perfusion. PM2 was further added together with thrombin (4 U mL^{-1}) upon cancer cell perfusion. Data analyzed by one-way ANOVA with Tukey's post hoc analysis for multiple comparisons (MDA-MB-231) and Student's *t*-test (MCF-7). Each datum point represents an individual device, with three ROIs imaged per device. Bars represent mean \pm SD. ns stands for not significant; $**P < 0.01$; $***P < 0.001$. Statistical analyses are described in the Experimental Section.

We have already shown that fibrin interactions with the endothelium results in endothelial barrier disruption (Figure 2f). Looser contacts between adjacent endothelial cells may allow cancer cells to transmigrate through the endothelium more readily, as seen in experiments where stimulation of the microvascular networks with tumor necrosis factor- α , known to increase endothelial permeability, significantly increased cancer cell extravasation rate.^[59] In addition, previous studies have shown that the interaction of fibrin with VE-cadherin leads to upregulated expression of ICAM-1 on the surface of endothelial cells.^[60,61] Finally, while recalcified plasma and cancer cells were introduced at the same time in the experiments presented here, future research could address the impact of thrombi on extravasation when introduced asynchronously with the cancer cells.

2.4. Effect of Thrombin on Cancer Cell Extravasation

To further investigate how the hypercoagulable state in cancer can enhance cancer cell extravasation, we sought to determine the effect of thrombin on the rate at which cancer cells extravasate. In a physiological state, there is little to no thrombin in the circulation, whereas the average concentration of prothrombin is $1400 \times 10^{-9} \text{ M}$.^[62] Upon activation of the coagulation cascade, Factor X rapidly generates the active form of thrombin from inactive prothrombin, which further gets amplified during the amplification phase of coagulation through positive feedback loops.^[63] The concentration of thrombin generated during this phase can range from $1 \times 10^{-9} \text{ M}$ (0.1 U mL^{-1}) to more than $500 \times 10^{-9} \text{ M}$ (50 U mL^{-1}).^[64] Several cancers have been associated with elevated blood levels of prothrombin fragments 1 + 2, peptides cleaved from prothrombin to generate active thrombin.^[65]

Besides the previously discussed effects of thrombin on the endothelium, evidence suggests that PAR-1 expression on cancer cells correlates with increased metastatic potential. In a 2D assay, thrombin was shown to stimulate breast cancer cell invasion in PAR-1-positive cell lines.^[66] In addition, Yang et al. showed that breast cancer cell lines either positive for PAR-1 or ectopically expressing it robustly metastasized to the lungs of mice, in comparison to PAR-1-negative breast cancer lines which did not form any metastases.^[67] We therefore asked whether thrombin enhances cancer cell extravasation in our system, acting through PAR-1 signaling. We again used MDA-MB-231, positive for PAR-1, and chose MCF-7, which do not express the receptor as a negative control.^[66] Surface expression of PAR-1 was first confirmed by flow cytometry (Figure 5a). Both cell lines were perfused through the microvascular networks, in the presence or absence of 4 U mL^{-1} thrombin in the perfused medium (Figure 5b). The thrombin concentration was increased here compared to the experiments used to quantify endothelial permeability, as thrombin has been shown to be significantly less stable at $37 \text{ }^\circ\text{C}$.^[68] Examining the confocal images, there is a higher proportion of MDA-MB-231 cells spreading, adhering to the endothelium, and subsequently extravasating upon thrombin stimulation. In addition, inhibiting PAR-1 using parmodulin-2 (PM2) significantly reduced extravasation. With the MCF-7 cells, thrombin seems to have much less of an effect, with most of them remaining round, as in the control samples. This is further reflected in the percentage of extravasated cells, which does not change upon thrombin stimulation, in contrast to the 2.8-fold increase seen in MDA-MB-231 cells (Figure 5c).

We have already shown that thrombin increases endothelial permeability (Figure 2g), which is expected to allow cancer cells to transmigrate through the endothelium more readily. In

addition, studies have shown that thrombin induces expression of adhesion molecules on the surface of endothelial cells, including P-selectin and ICAM-1. We have previously discussed how ICAM-1 can facilitate cancer cell extravasation, and P-selectin can also facilitate endothelial adhesion.^[69,70] In cancer cells, PAR-1 signaling has been shown to upregulate the expression of mesenchymal genes and downregulate the expression of epithelial genes, enhancing a more aggressive phenotype.^[67] Furthermore, besides thrombin, other molecules have been shown to activate PAR-1, including matrix metalloproteinase-2 (MMP-2), upregulated during network formation due to interstitial flow.^[35] Albeit not significant, the extravasation rate in networks treated with PM2 is slightly less than that seen in controls, a finding that could be explained by basal activation of PAR-1 in control samples through thrombin-independent mechanisms. Downstream of that, the variety of signaling pathways affected by PAR-1 activation that enhance cancer invasiveness are summarized by Liu et al.^[71] Besides the effects of thrombin on endothelial and cancer cells, thrombin has further been shown to upregulate C-C motif chemokine ligand 2 (CCL2) production by lung fibroblasts.^[72] In addition, a recent study demonstrated that CCL2 signaling enhanced cancer cell extravasation in an in vitro blood-brain barrier model through C-C chemokine receptor 2 (CCR2) signaling,^[73] a receptor expressed in both MDA-MB-231 and MCF-7 cell lines.^[74] The same signaling axis also been shown to correlate with a more invasive phenotype in patient-derived xenografts of breast cancer.^[75] It is thus possible this axis contributes to cancer cell extravasation in the system presented here. Nevertheless, the concentration of thrombin and duration of administration used here may be supraphysiologic, and future work could examine the timing and dose-dependence of thrombin exposure on extravasation in this model.

Taken together, our findings suggest that fibrinogen, fibrin, and thrombin all interact with cancer cells and enhance their extravasation rate. Thus, cancer cell line expression of cell-surface proteins such as ICAM-1 and PAR-1 enables differential metastatic potential through their interactions with fibrin(ogen) and thrombin. Our system enables more in-depth investigations of the interactions taking place between the coagulation system and cancer cells, and how those interactions affect cancer cell extravasation in turn.

3. Discussion

In this study, we have developed an in vitro model of clot formation in physiologically relevant microvascular networks, and used it to investigate how different components of the hypercoagulable state present in cancer affect endothelial function. We show that perfusion of recalcified plasma results in fibrin clot formation in the microvascular networks, the extent of which can be controlled by changing the concentration of plasma in medium. This model most closely resembles disseminated intravascular coagulation due to the systemic clotting in healthy vasculature that occurs when we perfuse recalcified plasma from phlebotomy blood draws rather than activation of the clotting cascade due to local damage to the endothelium. Fibrin thrombi contract within 24 hours, restoring flow past previously occluded segments. We further show that both fibrin and thrombin result in endothelial barrier disruption. Using this system, we have demonstrated

that breast cancer cells can transmigrate through the endothelium in a fibrinogen-dependent manner based on interactions with ICAM-1, and also interact with fibrin clots, which further enhance their extravasation rate. Lastly, we provide evidence that thrombin stimulation further enhances cancer cell extravasation, acting through its receptor PAR-1.

Regarding the impact fibrin thrombi have on endothelial barrier function, our data suggest that the interaction between fibrin through its B β 15-42 epitope and VE-cadherin^[76] results in disruption of barrier integrity. However, previously published studies present overall contrasting data, with some suggesting that this interaction increases endothelial permeability^[38] and some suggesting that it preserves barrier function.^[77,78] A more careful examination of the experimental methods of each study suggests that when B β 15-42 is part of the intact fibrin NDSK-II domain, its interaction with VE-cadherin induces endothelial hyperpermeability. However, upon plasmin-mediated fibrin degradation,^[79] the same epitope alone acts to protect endothelial barrier function, therefore providing a physiological feedback mechanism regulating vascular repair. Besides the interaction between fibrin with VE-cadherin however, other interactions of the fibrin clots with the endothelium could be present. Previous studies using our model have shown that within a week, key proteins of the basement membrane are deposited around the lumens formed, including collagen IV and laminin.^[59,80] Upon endothelial damage, which would trigger coagulation activation under physiological conditions, these proteins would be exposed, potentially mediating further interactions with fibrin. Laminin exposure would further allow cancer cell integrin β_1 to bind and facilitate migration into the subendothelial matrix.^[80]

Moreover, while in the present study we have only used breast cancer cell lines to study how ICAM-1 and PAR-1 receptors mediate interactions between the coagulation system and cancer cells, these mechanisms might be present among other types of metastatic cancer cells too. ICAM-1 overexpression has been reported in lung cancer, pancreatic cancer, and renal cell carcinoma among others, correlating to advanced risk of metastases.^[81–83] In addition, inhibiting the expression of the gene coding for ICAM-1 was shown to reduce invasion in a lung cancer model,^[84] and blocking the interaction of ICAM-1 and fibrinogen inhibited cell migration through HUVEC monolayers in a bladder transitional cell carcinoma model.^[85] PAR-1 has been shown to induce EMT following thrombin activation in gastric cancer cell lines,^[86] and to enhance adhesion, invasion and metastasis of melanoma cell lines.^[87] Overexpression of the receptor is also closely related to distant metastasis in multiple cancer cell lines.^[71] Taken together, these lines of evidence suggest that ICAM-1 and PAR-1 might be involved in enhancing the extravasation of circulating tumor cells originating from several types of primary tumors through interactions with the coagulation system.

In addition, besides the ICAM-1-dependent interaction that fibrinogen facilitates between cancer cells and the endothelium, studies have identified several other binding sites that could facilitate the same interaction. Endothelial cell integrins $\alpha_v\beta_3$ ^[88] and $\alpha_5\beta_1$ ^[89] can both bind to fibrinogen. Some cancer cells also express $\alpha_v\beta_3$,^[90] it is therefore possible that fibrinogen also bridges cancer cells to the endothelium through integrin-dependent mechanisms. Besides these fibrinogen-mediated linkages, direct interactions between cancer cell receptors and

endothelial ICAM-1 (upregulated by fibrin, IL-6,^[91] etc.) could also take place. Integrin β_2 can bind directly to ICAM-1, and expression of β_2 has been associated with several cancer cell lines.^[92] In addition, while fibrinogen is not present in our system after fibrin clot formation and reperfusion of vascular medium, this would not be the case in vivo. We could speculate that increased fibrin deposition in the hypercoagulable state of cancer leads to increased ICAM-1 presence on the endothelium, which can in turn be used by cancer cells to extravasate in a fibrinogen-dependent manner. Furthermore, the binding site of ICAM-1 on fibrinogen, a 17-amino-acid epitope on its γ chain,^[93] remains present on fibrin upon thrombin-mediated cleavage of fibrinopeptides A and B. It is therefore possible that the interaction with ICAM-1 occurs even following conversion of fibrinogen to fibrin. However, lateral aggregation of fibrin fibers could limit access to this binding site, while the orientation of the interacting epitopes could also disfavor their interaction, given that fibrin cannot move freely upon crosslinking.

Furthermore, we speculate that signaling between interleukin-8 (IL-8) and its receptor CXCR2 could be an important signaling axis in our system. Fibrinogen has been shown to upregulate IL-8 expression in synovial fibroblasts, mediated by NF- κ B activation;^[94] lung fibroblasts could potentially behave similarly. IL-8 signaling through CXCR2 was shown to increase colon cancer cell metastasis to the liver and lungs,^[95] as well as breast cancer cell metastasis to the thorax.^[96] The higher expression of CXCR2 in MDA-MB-231 compared to SKBR3 cells^[97] could contribute to the higher extravasation rate seen upon fibrinogen stimulation in MDA-MB-231 cells. Moreover, fibrin binding to endothelial cells has also been shown to stimulate IL-8 expression,^[98] further leading to enhanced extravasation in the presence of fibrin.

Nevertheless, the interactions investigated here constitute only a small fraction of the ways the coagulation system in cancer contributes to the extravasation of circulating tumor cells. As key components of the coagulation system, both red blood cells and platelets also have key roles in clot formation, contraction and eventually resolution. A recent study additionally demonstrated that platelets have key roles in remodeling the architecture of fibronectin in thrombi,^[99] which cancer cells have already been shown to interact with through integrin $\alpha_v\beta_3$ ^[56]—it is therefore reasonable to speculate that fibronectin architecture could affect cancer cell invasion of the thrombus. Furthermore, numerous studies have shown that platelets can facilitate cancer cell extravasation through transforming growth factor- β signaling, which upregulates expression of mesenchymal genes,^[100] recruitment of granulocytes, which promote transendothelial migration,^[101] and adenosine nucleotide secretion which induces endothelial barrier opening.^[102] In addition, it has previously been shown using in vitro microvascular networks that platelets enhance cancer cell extravasation, though this was not in the context of coagulation activation. Therefore, with key roles in both hemostasis and cancer cell extravasation, further studies incorporating platelets in our system would be of great interest, allowing in-depth investigation of primary hemostasis.

Immune cells are also key players in both thrombosis and metastatic dissemination. Neutrophils have been heavily implicated in both, through the secretion of neutrophil extracellular traps. These extracellular structures consist of chromatin

and other granular proteins, and can capture platelets and provide a scaffold for binding of other procoagulant molecules,^[103] while also contributing to the formation of premetastatic niches through increasing vascular permeability^[104] and inducing epithelial-to-mesenchymal transition (EMT) in circulating tumor cells.^[105] Monocytes are a source of TF, activating the extrinsic pathway of coagulation,^[106] while they also promote cancer cell extravasation through vascular endothelial growth factor signaling.^[107]

Beyond these cellular interactions, shear stress due to hemodynamic forces in circulation has also been linked to both thrombosis and cancer cell extravasation. Von Willebrand Factor has been shown to be shear-responsive, mediating platelet adhesion and aggregation differently in different flow regimes.^[108] Moreover, deposition of fibrin on the vessel walls can reduce the effective vessel diameter, increasing local shear stress, affecting in turn the distribution of platelets and red blood cells in the flow.^[109] Examining our data, fibrin fibers (Figure 2e) clearly follow flow-driven patterns, suggesting that the flow dynamics and by extension the 3D architecture of the microvascular network strongly impact clot formation patterns. Taken together, these studies provide concrete evidence of the fundamental role of hemodynamics on thrombus formation. Furthermore, past work has highlighted the effects of shear stress on cancer cell extravasation, showing a tendency for higher shear stresses to enhance cancer cell extravasation and subsequent tissue invasion.^[110,111] In light of this evidence, using our system to investigate the effects of both the coagulation system and shear stress on cancer cell extravasation, *combined*, could provide great insights into the interplay between different contributing factors.

The additional factors involved in thrombosis and metastasis (other cell–surface interactions, platelets, hemodynamics, etc.) can be incorporated in our system in future studies, to elucidate the interactions taking place between the coagulation system and cancer cells facilitating their extravasation.

4. Conclusion

In the present study, we have established a physiologically relevant in vitro model of clot formation in human lung microvasculature and showed different ways through which fibrinogen, fibrin, and thrombin regulate breast cancer cell extravasation. The versatility and accessibility of the platform can easily allow further investigation into the numerous parameters and interactions discussed throughout this work on cancer cell extravasation.

5. Experimental Section

Microfluidic Device Fabrication: The microfluidic devices used in this study were fabricated using polydimethylsiloxane (PDMS; Sylgard 184, Dow Corning, MI) with a central channel for the hydrogel/cell mixture and two adjacent fluidic channels for cell culture medium. The dimensions of the central gel channel were 3 mm width \times 8 mm length \times 0.5 mm height, except for the extravasation assays, where the height was 0.25 mm. Molds of the devices were designed in AutoCAD (Autodesk, Inc., CA, USA), and imported in Fusion 360 (Autodesk, Inc.) to generate corresponding tool paths, followed by milling a Delrin block with a micro-CNC milling machine (Bantam Tools). Elastomer and curing agent (10:1 mass ratio) were mixed, degassed, poured into the mold, and cured overnight at 60 °C.

Holes were created using biopsy punches, the devices were autoclaved, treated with oxygen plasma and bonded to sterilized glass coverslips. The devices were then placed in an oven at 70 °C for 2 d to restore hydrophobicity.

Cell Culture: Normal human lung fibroblasts (NHLFs, Lonza, CC-2512) and HUVECs (Lonza, CC-2935) were cultured in flasks coated with human gelatin (0.5% in phosphate buffer saline (PBS, Gibco, 10010031), Sigma, G1393) in either fibroblast medium (FibroLife S2 Fibroblast Medium Complete Kit, Lifeline Cell Technology LLC, LL-0011) or vascular medium (Vasculife VEGF Endothelial Medium Complete Kit, Lifeline Cell Technology LLC, LL-0003). HUVECs were immortalized and transfected to express blue fluorescent protein as described previously.^[112] Fibroblasts were used between passages 8 and 10 and endothelial cells were used between passages 10 and 12. MDA-MB-231 cells (ATCC, CRM-HTB-26), MFC-7 cells (ATCC, CRL-3435), and SKBR3 cells (ATCC, HTB-30) were cultured in Dulbecco's modified Eagle medium (DMEM, Gibco, 11995065) supplemented with 10% fetal bovine serum (FBS, Gibco, 26140079) and 1% penicillin/streptomycin (P/S, Gibco, 15140122). MDA-MB-231 cells were transfected to express tdTomato and MCF-7 and SKBR3 cells were transfected to express red fluorescent protein as described previously.^[113]

Microvascular Network Formation: NHLFs and HUVECs were detached using TrypLE (Gibco, 12604013), pelleted and resuspended in Vasculife with thrombin (4 U mL⁻¹, Sigma, T4648-1KU) at concentrations of 28×10^6 and 6×10^6 cells mL⁻¹, respectively. They were then mixed at equal volumes, and then mixed with an equal volume of fibrinogen in PBS solution (6 mg mL⁻¹, Sigma, 341578) and injected into the gel channel of each microfluidic device. The devices were placed for 10 min in a humidified incubator at 37 °C to allow the solution to polymerize, prior to addition of vascular medium in the side channels. Medium in these channels were changed daily, and after 3 d interstitial flows were introduced by connecting syringe tips cut at the 0.1 mL mark (BD, 309659) on one side of the gel channel as fluid reservoirs and applying a pressure drop of 1.5 cmH₂O.^[135] The networks were typically perfusable by day 7 and ready to be used in further experiments. For networks used in permeability analyses, endothelial monolayers were added in the side channels, to reduce dextran leakage through the sides of the central gel channel. On day 2, the side channels were coated with fibronectin (30 µg mL⁻¹, MilliporeSigma, FC010) in culture medium for 30 min, prior to incubation with HUVECs (1×10^6 cells mL⁻¹) for 5 min per side and subsequent return to medium.

Clot Generation and Image Analysis: Human plasma collected in sodium citrate (Research Blood Components LLC, #006) was spiked with fluorescent fibrinogen (0.06 mg mL⁻¹, Thermo Fisher, F13191 or F13192 depending on the experiment, 2% w/w assuming the average concentration of fibrinogen in the plasma of healthy individuals is 3 mg mL⁻¹^[40]) and filtered through a 0.2-µm filter (VWR International, 28145-501). Immediately before use, the plasma was recalcified using calcium chloride (final concentration of 10×10^{-3} M, Sigma, C-34006) to a and diluted to different concentrations in human plasma-like medium (HPLM, Gibco, A4899101). All reagents were kept on ice during use, and long-term storage was at -20 °C. Recalcified, fluorescent-spiked plasma solutions were perfused through the microvascular networks for 15 min before changing the medium back to vascular medium. Devices were then imaged right away. The percentage of fibrin⁺ vessel area and the fluorescent intensity of the corresponding areas were quantified using ImageJ (NIH, USA) from maximum intensity projection images. Fibrin⁺ was quantified following Renyi entropy thresholding. Finally, stitched images were produced using ImageJ's stitching plugin.^[114] For clots including platelets (Figure 1d), whole blood collected in sodium citrate (Research Blood Components LLC, #016) was centrifuged for 15 min at 120g, and the plasma and buffy coat layers were separated from the red blood cell layer. Platelets were labeled with a CD41 antibody (0.5 µg mL⁻¹, Biolegend, 303725) for 20 min at room temperature, and the resulting solution was diluted in PBS (1:4). Based on an average platelet concentration in whole blood of 3×10^8 platelets mL⁻¹, the final concentration of platelets in the coagulation assay is estimated to be 1.4×10^8 platelets mL⁻¹.^[24] Von Willebrand factor (vWF) was live-stained by combining unlabeled vWF monoclonal primary antibody (Invitrogen, MA5-14029) and a fluorescent secondary antibody (Life Technologies A21124), diluted 1:200 in medium. The antibody so-

lution was introduced into devices and incubated for 30 min before perfusing plasma and platelets. Upon perfusion through microvascular networks, stable clots were generated within 5 min, and devices were imaged immediately after.

Cancer Cell Perfusion and Extravasation Analysis: Breast cancer cells were detached using Accutase (Thermo Fisher, 00-4555-56). Cells were resuspended (2×10^6 cells mL⁻¹) in medium consisting of 50% DMEM (DMEM + 10% FBS + 1% P/S) and 50% vascular medium. Prior to perfusion, all medium was aspirated from the fluidic channels of the microfluidic devices. Cancer cell suspension (20 µL) was introduced to one of the fluidic channels, followed by culture medium (200 µL). Twice in 10-min intervals, the medium flowing through the microvascular networks to the fluidic channel on the opposite side of the central channel were aspirated. Parmodulin-2 (PM2) was purchased from MedChemExpress (HY-13965), and the ICAM-1 blocking antibody used was purchased from R&D Systems (BBA3). For the ICAM-1 experiments, fibrinogen was dissolved in culture medium for perfusion at a concentration of 3 mg mL⁻¹, aiming to mimic its concentration in human plasma.^[40] For the ICAM-1 blocking experiments, ICAM-1 was transiently knocked down in MDA-MB-231 cells before perfusion in microvascular networks also treated with the blocking antibody overnight (10 µg mL⁻¹). Lipofectamine RNAiMax (Thermo Fisher, 13778075) was used for siRNA transfection according to manufacturer recommendations. Briefly, 2×10^5 cells were plated in six-well plates 1 d before treatment with the transfection agent and siRNA against ICAM-1 (siRNA ID 105995 & 144513) or control (Silencer Negative Control #1 siRNA), all from Thermo Fisher. Knockdown was confirmed by flow cytometry (Figure S7, Supporting Information) as detailed in the following section. Cells were treated for 48 h before detachment with Accutase and perfusion through microvascular networks in the presence of 3 mg mL⁻¹ fibrinogen. For the PAR-1 inhibition experiments using PM2, both networks and cancer cells were treated for 4 h prior to perfusion (30×10^{-6} M), and PM2 was further added at the same concentration together with thrombin (4 U mL⁻¹). Culture medium was further changed once a day when extravasation experiments ran for longer than 24 h. Three regions of interest (ROIs) were imaged per device, and the average percentage of extravasated cells per device was determined. Each datum point represents one device. Cells were counted manually using ImageJ's Cell Counter plugin. When large clusters of cells were present, the number of cancer cells was estimated to the best of our ability based on cluster size. Cells in the process of extravasation were counted as extravasated. Only devices with more than 50 cancer cells in the microvascular networks were included in the final graphs.

Flow Cytometry and Analysis: Cells were grown to confluence, detached using Accutase and transferred to FACS tubes (Stellar Scientific, FSC-9005). They were then washed twice in PBS, before addition of conjugated primary antibodies or the corresponding isotype controls diluted 1:200 in FACS buffer (PBS supplemented with 2% FBS). The antibodies used were Alexa Fluor 488 CD54 (ICAM-1) (Biolegend, 322713) and corresponding isotype control (Biolegend, 400132) and Alexa Fluor 647 anti-human PAR1 (R&D Biosystems, FAB3855R) and corresponding isotype control (R&D Biosystems, IC0041R). The cells were incubated with the primary antibodies for 15 min, before another wash with FACS buffer and subsequent analysis using a BD FACSAria (BD Biosciences, CA, USA) flow cytometer. Analysis of flow cytometry data was performed using FlowJo v10 (Flexera Software, IL, USA).

Confocal Imaging, Perfusability, and Permeability Analyses: Images were acquired using an Olympus FV1000 (Olympus, Japan) confocal laser scanning microscope. Perfusability following fibrin thrombi formation was assessed by flowing fluorescent beads (1 µm diameter (Invitrogen, F8823), diluted 1:100 in PBS) through the microvascular networks. Vascular permeability was determined as previously described.^[36] Briefly, the networks were perfused with 70 kDa FITC-labeled dextran (Thermo Fisher, D1829) diluted in PBS (final concentration of 0.1 mg mL⁻¹). The dextran signal was imaged over several ROIs in each device at multiple timepoints. The vascular permeability was evaluated as the flux of solute across the walls of the vascular network using fluorescent intensity as a proxy for concentration. Using mass conservation, the quantity of fluorescently labeled dextran crossing the vascular network boundaries equals the rate at which

it accumulates in the extravascular region. The vascular permeability, P_v , was quantified by obtaining the average intensity of vessels (I_V) and tissue (outside vessels, I_T) at two different timepoints t_1 and t_2 and using Equation (1)

$$P_v = \frac{1}{(I_V^{t_1} - I_T^{t_1})} \frac{(I_T^{t_2} - I_T^{t_1})}{\Delta t} \frac{V}{A_{\text{surface}}} \quad (1)$$

Here, Δt is the time interval (in seconds) between the two images, V is the matrix volume in the ROI quantified, and A_{surface} is the surface area of all the vessels in the ROI. All the required parameters were computed using ImageJ after segmenting the vascular region and quantifying mean intensity, volume, and surface area of each class.

Statistical Analysis: All data are plotted as mean \pm SD, unless otherwise indicated. Each datum point corresponds to one ROI, except for extravasation experiments, where each datum point represents a device (average of three independent ROIs). In violin plots, midline indicates median, horizontal lines above and below indicate lower and upper quartiles. Sample size and number of independent experiments are indicated in each figure caption. 3D reconstructions for Figure S3 (Supporting Information) were generated using Imaris 7.4.2 (Oxford Instruments, UK). All statistical tests were performed using GraphPad Prism 8.0.2 (GraphPad Software, CA, USA). The ROUT test^[115] ($Q = 1\%$) was used to identify and remove outliers. The Shapiro–Wilk test was used to test whether the samples were normally distributed. Most samples did not follow a normal distribution, so the Mann–Whitney U test was used to compare between two conditions. When samples followed a normal distribution, the Student's t -test was used. Statistical tests are indicated in figure captions where performed, and these tests were two-tailed. When three conditions were compared (Figures 2f,g, 3c, and 5c), a one-way ANOVA with Tukey's post hoc analysis for multiple comparisons was applied. Significance was represented as follows: ns stands for not significant; * $P < 0.05$; ** $P < 0.01$; *** $P < 0.001$.

Supporting Information

Supporting Information is available from the Wiley Online Library or from the author.

Acknowledgements

Part of Figure 1 was created using Biorender.com. The authors thank the Swanson Biotechnology Center Flow Cytometry Facility at the Koch Institute for Integrative Cancer Research at MIT for technical support. The authors thank Dr. Kellie Machlus for advice regarding the establishment of the fibrin thrombi model. The authors thank Prof. Viola Vogel for helpful input and corrections of the manuscript. The authors also thank Dr. Mouhita Humayun for help with the micromilling machine used to generate the molds used in this study. The authors thank all members of the Mechanobiology Lab for helpful discussions during this project. The authors thank the MIT BioMicro Center, especially Charlie Demurjian and Stuart Levine, for support with data management. The MIT BioMicro Center was supported in part by the Koch Institute Support Grant (P30-CA14051) from the National Cancer Institute. E.A. acknowledges support by the Zeno Karl Schindler Foundation Master Thesis Grant. S.E.S. was supported by K00CA212227 from the NIH/NCI. This work was supported by the NIH grant U54CA261694 to R.D.K.

Conflict of Interest

R.D.K. is a co-founder and a board member of AIM Biotech. He also has current research support from Boehringer-Ingelheim, Roche, Amgen, GSK, and Novartis.

Data Availability Statement

The data that support the findings of this study are openly available in MIT Koch Institute BioMicro Center at <https://fairdomhub.org/studies/1133>, reference number 1133.

Keywords

cancer, coagulation, fibrin, metastasis, microphysiological systems

Received: November 17, 2022

Revised: April 25, 2023

Published online: May 12, 2023

- [1] A. A. Khorana, C. W. Francis, E. Culakova, N. M. Kuderer, G. H. Lyman, *J. Thromb. Haemostasis* **2007**, 5, 632.
- [2] N. B. A. Razak, G. Jones, M. Bhandari, M. C. Berndt, P. Metharam, *Cancers* **2018**, 10, 1.
- [3] D. P. Cronin-Fenton, F. Søndergaard, L. A. Pedersen, J. P. Fryzek, K. Cetin, J. Acquavella, J. A. Baron, H. T. Sørensen, *Br. J. Cancer* **2010**, 103, 947.
- [4] S. Sallah, J. Y. Wan, N. P. Nguyen, L. R. Hanrahan, G. Sigounas, *Thromb Haemost* **2001**, 86, 828.
- [5] R. L. Edwards, F. R. Rickles, T. E. Moritz, W. G. Henderson, L. R. Zacharski, W. B. Forman, C. J. Cornell, R. J. Forcier, J. F. O'Donnell, E. Headley, S. H. Kim, R. O'Dell, K. Tornyo, H. C. Kwaan, *Am. J. Clin. Pathol.* **1987**, 88, 596.
- [6] C. Ay, D. Dunkler, R. Pirker, J. Thaler, P. Quehenberger, O. Wagner, C. Zielinski, I. Pabinger, *Haematologica* **2012**, 97, 1158.
- [7] H. H. Versteeg, J. W. M. Heemsker, M. Levi, P. H. Reitsma, *Physiol. Rev.* **2013**, 93, 327.
- [8] T. Riedel, J. Suttner, E. Brynda, M. Houska, L. Medved, J. E. Dyr, *Blood* **2011**, 117, 1700.
- [9] O. V. Kim, R. I. Litvinov, M. S. Alber, J. W. Weisel, *Nat. Commun.* **2017**, 8, 1.
- [10] T. G. Diacovo, S. J. Roth, J. M. Buccola, D. F. Bainton, T. A. Springer, *Blood* **1996**, 88, 146.
- [11] B. Scheuerer, M. Ernst, I. Dürbaum-Landmann, J. Fleischer, E. Grage-Griebenow, E. Brandt, H. D. Flad, F. Petersen, *Blood* **2000**, 95, 1158.
- [12] G. Elyamany, A. M. Alzahrani, E. Bukhary, *Clin. Med. Insights: Oncol.* **2014**, 8, 129.
- [13] D. Hanahan, R. A. Weinberg, *Cell* **2011**, 144, 646.
- [14] J. S. Palumbo, K. W. Kombrinck, A. F. Drew, T. S. Grimes, J. H. Kiser, J. L. Degen, T. H. Bugge, *Blood* **2000**, 96, 3302.
- [15] E. Camerer, A. A. Qazi, D. N. Duong, I. Cornelissen, R. Advincula, S. R. Coughlin, *Blood* **2004**, 104, 397.
- [16] J. S. Palumbo, K. E. Talmage, J. V. Massari, C. M. La Jeunesse, M. J. Flick, K. W. Kombrinck, Z. Hu, K. A. Barney, J. L. Degen, *Blood* **2007**, 110, 133.
- [17] Y. Zheng, J. Chen, M. Craven, N. W. Choi, S. Totorica, A. Diaz-Santana, P. Kermani, B. Hempstead, C. Fischbach-Teschl, J. A. López, A. D. Stroock, *Proc. Natl. Acad. Sci. USA* **2012**, 109, 9342.
- [18] Y. S. Zhang, F. Davoudi, P. Walch, A. Manbachi, X. Luo, V. Dell'Erba, A. K. Miri, H. Albadawi, A. Arneri, X. Li, X. Wang, M. R. Dokmeci, A. Khademhosseini, R. Oklu, *Lab Chip* **2016**, 16, 4097.
- [19] Y. Sakurai, E. T. Hardy, B. Ahn, R. Tran, M. E. Fay, J. C. Ciciliano, R. G. Mannino, D. R. Myers, Y. Qiu, M. A. Carden, W. H. Baldwin, S. L. Meeks, G. E. Gilbert, S. M. Jobe, W. A. Lam, *Nat. Commun.* **2018**, 9, 1.
- [20] J. D. Crissman, J. S. Hatfield, D. G. Menter, B. Sloane, K. V. Honn, *Cancer Res.* **1988**, 48, 4065.

- [21] I. J. Fidler, *Nat. Rev. Cancer* **2003**, *3*, 453.
- [22] M. B. Chen, J. A. Whisler, J. Fröse, C. Yu, Y. Shin, R. D. Kamm, *Nat. Protoc.* **2017**, *12*, 865.
- [23] S. Palta, R. Saroa, A. Palta, *Indian J. Anaesth.* **2014**, *58*, 515.
- [24] B. J. Bain, *Blood Cells: A Practical Guide*, Wiley-Blackwell, Hoboken, NJ **2015**.
- [25] D. B. Cines, T. Lebedeva, C. Nagaswami, V. Hayes, W. Massefski, R. I. Litvinov, L. Rauova, T. J. Lowery, J. W. Weisel, *Blood* **2014**, *123*, 1596.
- [26] C. Wloka, E. A. Vallen, L. Thé, X. Fang, Y. Oh, E. Bi, *J. Cell Biol.* **2013**, *200*, 271.
- [27] Z. Xue, A. M. Sokac, *J. Cell Biol.* **2016**, *215*, 335.
- [28] S. Chen, T. Markovich, F. C. MacKintosh, **2022**, <http://arxiv.org/abs/2204.00222>.
- [29] R. I. Litvinov, J. W. Weisel, *Matrix Biol.* **2017**, *60*, 110.
- [30] A. Montero, S. Acosta, R. Hernández, C. Elvira, J. L. Jorcano, D. Velasco, *J. Biomed. Mater. Res., Part A* **2021**, *109*, 500.
- [31] L. Zhang, D. Seiffert, B. J. Fowler, G. R. Jenkins, T. C. Thinnies, D. J. Loskutoff, R. J. Parmer, L. A. Miles, *Thromb. Haemostasis* **2002**, *87*, 493.
- [32] A. Mauro, M. Buscemi, A. Gerbino, *J. Mol. Histol.* **2010**, *41*, 367.
- [33] Y. Hojo, U. Ikeda, M. Takahashi, Y. Sakata, T. Takizawa, K. Okada, T. Saito, K. Shimada, *J. Mol. Cell. Cardiol.* **2000**, *32*, 1459.
- [34] K. Y. Han, J. H. Chang, H. Lee, D. T. Azar, *Invest. Ophthalmol. Visual Sci.* **2016**, *57*, 3313.
- [35] S. Zhang, Z. Wan, G. Pavlou, A. X. Zhong, L. Xu, R. D. Kamm, *Adv. Funct. Mater.* **2022**, <https://doi.org/10.1002/adfm.202206767>.
- [36] G. S. Offeddu, K. Haase, M. R. Gillrie, R. Li, O. Morozova, D. Hickman, C. G. Knutson, R. D. Kamm, *Biomaterials* **2019**, *212*, 115.
- [37] T. L. Bach, C. Barsigian, C. H. Yaen, J. Martinez, *J. Biol. Chem.* **1998**, *273*, 30719.
- [38] A. Sahni, M. T. Afevalo, S. K. Sahni, P. J. Simpson-Haidaris, *Int. J. Cancer* **2009**, *125*, 577.
- [39] M. J. Rabiet, J. L. Plantier, Y. Rival, Y. Genoux, M. G. Lampugnani, E. Dejana, *Arterioscler., Thromb., Vasc. Biol.* **1996**, *16*, 488.
- [40] M. Pieters, A. S. Wolberg, *Res. Pract. Thromb. Haemostasis* **2019**, *3*, 161.
- [41] C. S. D. Roxburgh, D. C. McMillan, *Br. J. Cancer* **2014**, *110*, 1409.
- [42] T. Yamaguchi, Y. Yamamoto, S. Yokota, M. Nakagawa, M. Ito, T. Ogura, *Jpn. J. Clin. Oncol.* **1998**, *28*, 740.
- [43] L. Kozłowski, I. Zakrzewska, P. Tokajuk, M. Z. Wojtukiewicz, *Rocz. Akad. Med. Białymstoku* **2003**, *48*, 82.
- [44] J. V. Castell, M. J. Gómez-Lechón, M. David, T. Andus, T. Geiger, R. Trullenque, R. Fabra, P. C. Heinrich, *FEBS Lett.* **1989**, *242*, 237.
- [45] A. Sahni, P. J. Simpson-haidaris, S. K. Sahni, G. G. Vaday, C. W. Francis, *J. Thromb. Haemostasis* **2008**, *6*, 176.
- [46] X. Zhang, Q. Long, *Med* **2017**, <http://dx.doi.org/10.1097/MD.0000000000006694>.
- [47] X. Yu, F. Hu, Q. Yao, C. Li, H. Zhang, Y. Xue, *BMC Cancer* **2016**, *16*, 1.
- [48] Y. Zhang, J. Cao, Y. Deng, Y. Huang, R. Li, G. Lin, M. Dong, Z. Huang, *Clinics* **2020**, *75*, 1.
- [49] C. Huang, N. Li, Z. Li, A. Chang, Y. Chen, T. Zhao, Y. Li, X. Wang, W. Zhang, Z. Wang, L. Luo, J. Shi, S. Yang, H. Ren, J. Hao, *Nat. Commun.* **2017**, <https://doi.org/10.1038/ncomms14035>.
- [50] P. Guo, J. Huang, L. Wang, D. Jia, J. Yang, D. A. Dillon, D. Zurakowski, H. Mao, M. A. Moses, D. T. Auguste, R. Langer, *Proc. Natl. Acad. Sci. USA* **2014**, *111*, 14710.
- [51] R. Sumagin, E. Lomakina, I. H. Sarelius, *Am. J. Physiol.* **2008**, *295*, H969.
- [52] S. Etienne-Manneville, N. Chaverot, A. D. Strosberg, P. O. Couraud, *J. Immunol.* **1999**, *163*, 668.
- [53] F. X. Bosch, J. Ribes, M. Díaz, R. Cléries, *Gastroenterology* **2004**, *127*, 5.
- [54] H. Dai, H. Zhou, Y. Sun, Z. H. E. Xu, S. Wang, T. Feng, P. Zhang, *Biomed. Rep.* **2018**, *9*, 453.
- [55] G. Malik, L. M. Knowles, R. Dhir, S. Xu, S. Yang, E. Ruoslahti, J. Pilch, *Cancer Res.* **2010**, *70*, 4327.
- [56] L. M. Knowles, L. A. Gurski, C. Engel, J. R. Gnarra, J. K. Maranchie, J. Pilch, *Cancer Res.* **2013**, *73*, 6175.
- [57] D. Shechter, M. Harel, A. Mukherjee, L. M. Sagredo, D. Loven, E. Prinz, S. Avraham, V. Orian-Rousseau, T. Geiger, Y. Shaked, H. Wolfenson, *Cells* **2020**, <https://doi.org/10.3390/cells9102269>.
- [58] C. Zhang, Z. Yang, P. Zhou, M. Yu, B. Li, Y. Liu, J. Jin, W. Liu, H. Jing, J. Du, J. Tian, Z. Zhao, J. Wang, Y. Chu, C. M. Zhang, V. A. Novakovic, J. Shi, C. Wu, *Theranostics* **2021**, *11*, 6445.
- [59] M. B. Chen, J. A. Whisler, J. S. Jeon, R. D. Kamm, *Integr. Biol.* **2013**, *5*, 1262.
- [60] J. Qi, D. L. Kreutzer, T. H. Piela-Smith, *J. Immunol.* **1997**, *158*, 1880.
- [61] S. L. Harley, J. Sturge, J. T. Powell, *Arterioscler., Thromb., Vasc. Biol.* **2000**, *20*, 652.
- [62] S. Butenas, K. G. Mann, *Biochemistry* **2002**, *67*, 3.
- [63] T. Madhusudhan, B. A. Kerlin, B. Isermann, *Nat. Rev. Nephrol.* **2016**, *12*, 94.
- [64] G. A. Allen, A. S. Wolberg, J. A. Oliver, M. Hoffman, H. R. Roberts, D. M. Monroe, *J. Thromb. Haemostasis* **2004**, *2*, 402.
- [65] M. Z. Wojtukiewicz, M. Rucinska, L. Zimnoch, J. Jaromin, Z. Piotrowski, M. Rózanska-Kudelska, W. Kisiel, B. J. Kudryk, *Thromb. Res.* **2000**, *97*, 335.
- [66] K. Henrikson, S. Salazar, J. Fenton II, B. Pentecost, *Br. J. Cancer* **1999**, *79*, 401.
- [67] E. Yang, J. Cisowski, N. Nguyen, K. O. Callaghan, J. Xu, A. Agarwal, A. Kuliopulos, L. Covic, *Oncogene* **2015**, *1*, 1529.
- [68] V. Kumar, T. Madsen, H. Zhu, E. Semple, *J. Extra-Corpor. Technol.* **2005**, *37*, 390.
- [69] M. E. Reyes-Reyes, M. D. George, J. D. Roberts, S. K. Akiyama, *Exp. Cell Res.* **2006**, *312*, 4056.
- [70] U. Richter, C. Schröder, D. Wicklein, T. Lange, S. Geleff, V. Dippel, U. Schumacher, S. Klutmann, *Histochem. Cell Biol.* **2011**, *135*, 499.
- [71] X. Liu, J. Yu, S. Song, X. Yue, Q. Li, *OncoTargets Ther.* **2017**, *8*, 107334.
- [72] A. Ortiz-Stern, X. Deng, N. Smoktunowicz, P. F. Mercer, R. C. Chambers, *J. Cell. Physiol.* **2012**, *227*, 3575.
- [73] C. Hajal, Y. Shin, L. Li, J. C. Serrano, T. Jacks, R. D. Kamm, *Sci. Adv.* **2021**, *7*, 1.
- [74] Y. Lu, Z. Cai, G. Xiao, Y. Liu, E. T. Keller, Z. Yao, J. Zhang, *J. Cell. Biochem.* **2007**, *101*, 676.
- [75] W. Bin Fang, D. Sofia Acevedo, C. Smart, B. Zinda, N. Alissa, K. Warren, G. Fraga, L. C. Huang, Y. Shyr, W. Li, L. Xie, V. Staggs, Y. Hong, F. Behbod, N. Cheng, *Sci. Rep.* **2021**, *11*, 1.
- [76] S. Yakovlev, L. Medved, *Biochemistry* **2009**, *48*, 5171.
- [77] M. Gröger, W. Pasteiner, G. Ignatyev, U. Matt, S. Knapp, A. Atrasheuskaya, E. Bukin, P. Freidl, D. Zinkl, R. Hofer-Warbinek, K. Zacharowski, P. Petzelbauer, S. Reingruber, *PLoS One* **2009**, *4*, 5391.
- [78] S. Yakovlev, C. Cao, R. Galisteo, L. Zhang, D. K. Strickland, L. Medved, *Thromb. Haemostasis* **2019**, *119*, 1816.
- [79] P. Petzelbauer, P. A. Zacharowski, Y. Miyazaki, P. Friedl, G. Wickenhauser, F. J. Castellino, M. Gröger, K. Wolff, K. Zacharowski, *Nat. Med.* **2005**, *11*, 298.
- [80] M. B. Chen, J. M. Lamar, R. Li, R. O. Hynes, R. D. Kamm, *Cancer Res.* **2016**, *76*, 2513.
- [81] Y. C. Lin, C. T. Shun, M. S. Wu, C. C. Chen, *Clin. Cancer Res.* **2006**, *12*, 7165.
- [82] A. A. Tempia-Caliera, L. Z. Horvath, A. Zimmermann, T. T. Tihanyi, M. Korc, H. Friess, M. W. Büchler, *J. Surg. Oncol.* **2002**, *79*, 93.
- [83] B. Hemmerlein, J. Scherbening, A. Kugler, H. J. Radzun, *Histopathology* **2000**, *37*, 78.
- [84] W. C. Huang, S. T. Chan, T. L. Yang, C. C. Tzeng, C. C. Chen, *Carcinogenesis* **2004**, *25*, 1925.

- [85] Y. Roche, D. Pasquier, J. J. Rambeaud, D. Seigneurin, A. Duperray, *Thromb. Haemostasis* **2003**, *89*, 1089.
- [86] L. Pang, J. fang Li, L. Su, M. Zang, Z. Fan, B. Yu, X. Wu, C. Li, M. Yan, Z. G. Zhu, B. Liu, *J. Gastroenterol.* **2018**, *53*, 71.
- [87] M. Zigler, T. Kamiya, E. C. Brantley, G. J. Villares, M. Bar-Eli, *Cancer Res.* **2011**, *71*, 6561.
- [88] D. A. Cheresh, S. A. Berliner, V. Vicente, Z. M. Ruggeri, *Cell* **1989**, *58*, 945.
- [89] K. Suehiro, J. Gailit, E. F. Plow, *J. Biol. Chem.* **1997**, *272*, 5360.
- [90] E. K. Sloan, N. Pouliot, K. L. Stanley, J. Chia, J. M. Moseley, D. K. Hards, R. L. Anderson, *Breast Cancer Res.* **2006**, *8*, 1.
- [91] B. S. Wung, C. W. Ni, D. L. Wang, *J Biomed Sci* **2005**, *12*, 91.
- [92] A. Benedicto, J. Marquez, A. Herrero, E. Olaso, E. Kolaczowska, B. Arteta, *BMC Cancer* **2017**, *17*, 1.
- [93] S. E. D'Souza, V. J. Byers-Ward, E. E. Gardiner, H. Wang, S. S. Sung, *J. Biol. Chem.* **1996**, *271*, 24270.
- [94] X. Liu, T. H. Piela-Smith, *J. Immunol.* **2000**, *165*, 5255.
- [95] Y. S. Lee, I. Choi, Y. Ning, N. Y. Kim, V. Khatchadourian, D. Yang, H. K. Chung, D. Choi, M. J. Labonte, R. D. Ladner, K. C. N. Venkata, D. O. Rosenberg, N. A. Petasis, H. J. Lenz, Y. K. Hong, *Br. J. Cancer* **2012**, *106*, 1833.
- [96] K. Jin, N. B. Pandey, A. S. Popel, *Oncotargets Ther.* **2017**, *8*, 60210.
- [97] B. Sharma, D. M. Nawandar, K. C. Nannuru, M. L. Varney, R. K. Singh, *Mol. Cancer Ther.* **2013**, *12*, 799.
- [98] J. Qi, S. Goralnick, D. L. Kreutzer, *Blood* **1997**, *90*, 3595.
- [99] S. Lickert, M. Kenny, K. Selcuk, J. L. Mehl, M. Bender, S. M. Früh, M. A. Burkhardt, J. Studt, B. Nieswandt, I. Schoen, V. Vogel, *Sci. Adv.* **2022**, *8331*, 1.
- [100] M. Labelle, S. Begum, R. O. Hynes, *Cancer Cell* **2011**, *20*, 576.
- [101] M. Labelle, S. Begum, R. O. Hynes, *Proc. Natl. Acad. Sci. USA* **2014**, *111*, E3053.
- [102] D. Schumacher, B. Strilic, K. K. Sivaraj, N. Wettschureck, S. Offermanns, *Cancer Cell* **2013**, *24*, 130.
- [103] C. Thâlin, Y. Hisada, S. Lundström, N. Mackman, H. Wallén, *Arterioscler., Thromb., Vasc. Biol.* **2019**, *39*, 1724.
- [104] Y. Ma, X. Yang, V. Chatterjee, J. E. Meegan, R. S. Beard, S. Y. Yuan, *Front. Immunol.* **2019**, *10*, 1.
- [105] E. Pieterse, N. Rother, M. Garsen, J. M. Hofstra, S. C. Satchell, M. Hoffmann, M. A. Loeven, H. K. Knaapen, O. W. H. Van Der Heijden, J. H. M. Berden, L. B. Hilbrands, J. Van Der Vlag, *Arterioscler., Thromb., Vasc. Biol.* **2017**, *37*, 1371.
- [106] C. Schulz, B. Engelmann, S. Massberg, *J. Thromb. Haemostasis* **2013**, *11*, 233.
- [107] B. Z. Qian, J. Li, H. Zhang, T. Kitamura, J. Zhang, L. R. Campion, E. A. Kaiser, L. A. Snyder, J. W. Pollard, *Nature* **2011**, *475*, 222.
- [108] Z. M. Ruggeri, J. N. Orje, R. Habermann, A. B. Federici, A. J. Reininger, *Blood* **2006**, *108*, 1903.
- [109] K. S. Sakariassen, L. Orning, V. T. Turitto, *Future Sci. OA* **2015**, <https://doi.org/10.4155/fso.15.28>.
- [110] C. Hajal, L. Ibrahim, J. C. Serrano, G. S. Offeddu, R. D. Kamm, *Biomaterials* **2021**, *265*, 120470.
- [111] S. Ma, A. Fu, G. G. Y. Chiew, K. Q. Luo, *Cancer Lett.* **2017**, *388*, 239.
- [112] Z. Wan, S. Zhang, A. X. Zhong, S. E. Shelton, M. Campisi, S. K. Sundararaman, G. S. Offeddu, E. Ko, L. Ibrahim, M. F. Coughlin, T. Liu, J. Bai, D. A. Barbie, R. D. Kamm, *Biomaterials* **2021**, *276*, 121032.
- [113] G. S. Offeddu, C. Hajal, C. R. Foley, Z. Wan, L. Ibrahim, M. F. Coughlin, R. D. Kamm, *Commun. Biol.* **2021**, *4*, 1.
- [114] S. Preibisch, S. Saalfeld, P. Tomancak, *Bioinformatics* **2009**, *25*, 1463.
- [115] H. J. Motulsky, R. E. Brown, *BMC Bioinf.* **2006**, *7*, 1.